Lasers in Surgery and Medicine 21:227–234 (1997)

Three-Dimensional Optical Phantom and Its Application in Photodynamic Therapy

Roland Bays, PhD,[1]* Georges Wagnières, PhD,[1] Dimitri Robert, BS,[1] Jean-François Theumann, PhD,[1] Alex Vitkin, PhD,[3] Jean-François Savary, MD,[2] Philippe Monnier, MD,[2] and Hubert van den Bergh, PhD[1]

[1]Institute of Environmental Engineering, Swiss Federal Institute of Technology, CH-1015 Lausanne, Switzerland
[2]ENT Department, CHUV Hospital, CH-1011 Lausanne, Switzerland
[3]Medical Physics, Ontario Cancer Institute, Toronto, Ontario M5G 2M9, Canada

Background and Objective: **A technique to manufacture a stable, reproducible three-dimensional optical phantom is presented. This phantom reproduces the tissue's optical properties as well as the geometry and, to some extent, the mechanical properties of the organ concerned. Easy to make and to handle, this phantom is a useful tool for numerous medical applications involving light interaction with biological tissues.**
Study Design/Materials and Methods: **The phantom is based on a transparent two-component silicone, which is molded into the desired shape and cured at room temperature. Specific optical properties are obtained by adding scatterers (Al_2O_3 particles or polystyrene microspheres) and absorbers (dyes or pigments). A method to measure the radiant energy fluence rate in the phantom is described. This method is based on a small isotropic optical detector.**
Results: **A three-dimensional phantom of the bronchial tree is presented. This phantom is used for testing new light distributors designed for photodynamic therapy of the bronchi.**
Conclusion: **The proposed technique allows one to produce a stable three-dimensional phantom with accurately predictable optical properties. Lasers Surg. Med. 21:227–234, 1997.**

Key words: laser tissue interaction; light dosimetry; optical properties; PDT; photomedicine; tissue optics

INTRODUCTION

Photodynamic therapy [1–4] (PDT) is a minimally invasive technique that can effectively treat superficial early cancers in the pharynx, esophagus, and tracheo-bronchial tree. This therapy is generally based on the selective localization of an i.v. dye in neoplastic tissues, followed by irradiation of the tumor and its immediate surroundings with visible light. Phototoxic properties of the dye then facilitate the selective destruction of tumors. At present, clinically used photosensitizers appear to have insufficient selectivity for PDT. This lack of selectivity may result in significant damage to the healthy tissue during the photodynamic treatment of the tumor. Since the therapeutic effect depends partly on the radiant energy density [J/cm^3] absorbed by the photosensitizer, the effects of insufficient selectivity must not be rendered worse by inaccurate light delivery.

In order to obtain appropriate light delivery during photodynamic treatment, it is necessary to develop a suitable light diffuser for each site geometry to be treated. An optimal light source would deliver light only to the tumor. In the pharynx, esophagus, and tracheo-bronchial tree, early cancers present superficial, often multicentric

*Correspondence to: R. Bays, Ph.D., Institute of Environmental Engineering, Swiss Federal Institute of Technology, CH-1015, Lausanne, Switzerland.

Accepted 29 May 1996

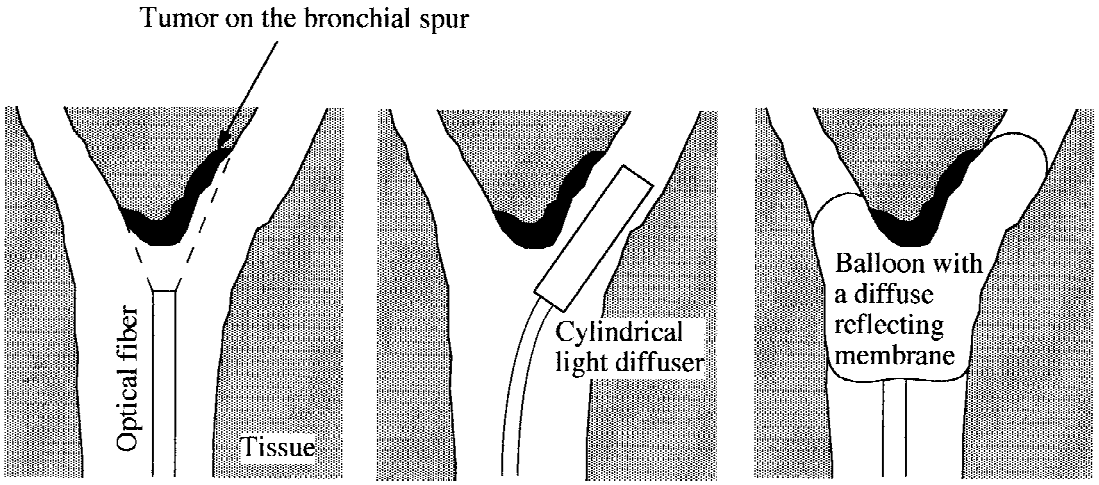

Fig. 1. Possible light diffuser geometries for PDT in the tracheo-bronchial tree: frontal illumination [5], cylindrical light diffuser [5–7], and soft balloon diffuser [8]. In the latter, the light, guided by an optical fiber, is emitted inside an air filled latex balloon. The soft balloon, with its partially reflecting walls, acts as an intregrating sphere and provides a relatively homogeneous illumination at the tissue surface.

and multifocal lesions. Under these conditions, an optimal delivery is difficult to achieve and a light source that provides as much or more light to the tumor than to the surrounding tissue, must often suffice. For the esophagus, a cylindrical light distributor [5,6] has been developed with different diameters, generally of the order of 15 mm. Such a diameter is suited to distend and to smooth the esophagus wall surface. This light source, in contact with a diffusing medium such as living tissue, delivers light uniformly to the surface of the organ. With this simple cylindrical site geometry and the uniform light distribution, it is possible to obtain a well controlled distribution of the radiant energy fluence rate in the esophageal walls.

In the bronchial tree, the geometry of the sites to be treated is more complex. Typically, the carcinoma appears on or near the bronchial spurs (see Fig. 1). To homogeneously illuminate the bronchial mucosa at this type of site, several solutions have been proposed [5–8] (some of which are shown in Fig. 1). Regardless of the illumination method, it is difficult to predict the light intensity distribution in the tumor and in the surrounding tissue from the tissue's optical properties, from the characteristics of the light distributor, as well as from the site geometry and the position of the light source at this site. Before using a new light distributor in PDT, one must be sure that the amount of light delivered to the entire treatment site will not induce medical complications such as fistula (organ perforation). Also, the light distribution should not be too sensitive to the light distributor positioning near the site, whatever the site geometry. In order to assess the quality of new light distributors for PDT in the lung, we have developed a three-dimensional optical phantom of this organ. A very small isotropic light detector can be introduced into this phantom at several strategic positions to measure the radiant energy fluence rate. This phantom can also be used by physicians to practice the introduction and placement of the light distributor for PDT in the tracheo-bronchial tree.

In this article, we present the technique of making three-dimensional phantoms and we show how the desired optical properties at the wavelength of interest are attained.

MATERIALS AND METHODS

The Basic Material

The basic transparent medium consists of a high-strength two-component room temperature curing silicone (Rhodorsil RTV 141, Rhône-Poulenc, France). The base and the catalyst are mixed at a ratio of one part catalyst to 10 parts of base by weight. To avoid air entrapment, it is sometimes necessary, especially in bulky phantoms, to subject the mixture to a vacuum. We found a pressure of 685 mm Hg to be adequate. However, the vacuum is often not necessary since the bubbles have time during the curing process to disappear by migrating to the surface of the phantom. Once the components are mixed, curing begins throughout the material. In 24 hours, the curing is sufficient

to permit handling, but full mechanical properties are developed only after 3 to 5 days. Heat can be applied to accelerate the curing, but higher shrinkage will result.

Before curing, the matrix material has a relatively low viscosity (4,000 cP) and can be easily used for molding. After curing, the silicone mechanical properties give the phantom a consistency close to that observed with some soft tissues. In numerous applications, the characteristics of a new optical device to be tested or calibrated are determined by the optical interface, which itself depends on the mechanical properties of the sample. In this way, silicone is more appropriate than harder materials such as polyester plastics [9].

Optical Properties

The silicone base material is transparent with a refractive index of about 1.4. The refractive index of soft tissues has been reported to be between 1.35 and 1.5 [10]. Different absorption, fluorescence, and scattering properties can be attained by adding chromophores, fluorophores, and scattering particles to the transparent matrix. To obtain a spatially homogeneous distribution of these various components in the silicone, the following technique was used. The component is first dissolved or dispersed in ethanol and the solution is carefully mixed with the silicone base. Ethanol is then removed by evaporation either in a fumehood or by gentle heating. Finally, after allowing the base to cool, the catalyst is added and the curing process can take place. Methanol, dimethyl sulphoxide (DMSO), and water have also been used successfully as solvents or dispersants instead of ethanol. The same technique of evaporation has been performed to remove these before the curing. Water appeared to be the most difficult liquid to mix with silicone and a homogeneous distribution of dye in the phantom was obtained only after complete evaporation of the water. Other solvents can certainly be used, but have not been tested so far.

In order to yield the required scattering properties, Al_2O_3 particles and polystyrene microspheres were used. Al_2O_3 particles, which are less expensive than the microspheres, are easy to mix with the silicone and result in a homogeneous distribution of scatterer. But low concentration of the particles has been observed on the first 100 microns of the phantom's surface. In numerous applications such as the lung phantom shown hereafter, this "skin effect" may be neglected. But in the case of thin tissue phantoms or stratified tissue phantoms where layers are only a few hundred microns thick, this effect is unacceptable. For this reason, polystyrene microspheres with diameters of 1.6 μm and 4 μm have been tested.[1] No phantom inhomogeneity has been observed so far with these particles. Moreover, Mie theory is well suited for these spherical and equal-sized particles. The scattering properties of Al_2O_3 particles, in spite of their irregular shape and their broad size distribution, can also be estimated with Mie theory. As an example, Al_2O_3 particles used in the lung phantom have an approximately gaussian size distribution defined by a mean value of 9.3 μm and a standard deviation of 4.6 μm. From Mie theory applied to a size distribution of scatterers [11,12], the predicted values for the scattering coefficient μ_s and the anisotropy parameter g at 633 nm are 2.46 mm^{-1} and 0.88 respectively, with a concentration of particles in the phantom of 4% by weight. The scattering coefficient μ_s [mm^{-1}] is defined so that $1\text{-}e^{-\mu s\, z}$ is the probability for a photon to be scattered in the pathlength z and g is the average cosine of the scattering angle. Typical values of g for soft tissue and 500–900 nm light vary between 0.7 and 0.99 [14]. The effective scattering coefficient $\mu'_s = \mu_s (1 - g)$ of the lung phantom was measured as 0.35 mm^{-1} by a non-invasive technique based on the measurement of the diffuse reflectance [15,16]. The predicted value was 0.3 mm^{-1}. The non-spherical shape of the Al_2O_3 particles is one reason for the discrepancy between prediction and measurement. Another source of error is the size distribution of these particles which has been approximated by a gaussian distribution. The relative accuracy of the measurement technique is another possible cause. Further investigations are underway to test the accuracy of the prediction for both Al_2O_3 and polystyrene particles.

Absorption properties were obtained by adding a dye or a pigment to the silicone. In the case of the lung phantom, in order to mimic the tissue optical properties for one wavelength (i.e., 630

[1]The 4 μm polystyrene particles (powder form) were a gift from Dr. Anthony James Paine at Xerox Research Centre of Canada [13] and the 1.6 μm polystyrene particles dispersed in ethanol were provided by Dr. Harald Stover and Mr. Jeff Downey, Department of Chemistry, McMaster University, Hamilton, Canada. The 1.6 μm particles can also be obtained from Interact Polymer Group, 135 Haddon St. South, Hamilton ON L8S 1X7, Canada.

nm), colloidal graphite dispersed in ethanol was used.

Preliminary trials were performed to mix blood and silicone. The result was homogeneous and stable over the time. More studies have to be done to determine the resulting optical properties of this phantom.

An optically heterogeneous medium, such as a layered structure, can also be obtained. Optically homogeneous parts have to be cured and added one after the other. In this way, good optical and mechanical contact is insured between each part of the phantom.

Shape

Several techniques can be used to obtain the organ shape. Molding is especially suitable with silicone. To produce the lung phantom, a negative imprint of the tracheo-bronchial tree was cast in wax (Fig. 2). This imprint was immersed in the silicone. After curing, the wax was removed by melting. With this technique, three-dimensional shapes can be accurately produced with only one mold (Fig. 3). Some other molding materials such as Alginate (used in dentistry) are non-toxic for skin and mucous, and they can therefore be used to produce body molds.

Radiant Energy Fluence Rate Measurement

In order to perform radiant energy fluence rate measurements, several narrow tunnels in the phantom (Fig. 4) allow small isotropic detectors to be introduced at several well-defined positions. The end of each tunnel, which corresponds to the measurement position, is the same distance from the surface of the bronchial tree. These tunnels were obtained by accurately positioning steel rods around the wax negative imprint before immersing it in the silicone (Fig. 5). After curing, the steel rods were withdrawn. In order to facilitate the introduction of the isotropic probe and to ensure an optical index match between the probe and the phantom, tunnels are filled with glycerin ($n = 1.475$). The refractive index of surrounding material affects the probe responsivity [16] and has to be carefully controlled.

The isotropic probe was previously developed for in vivo measurements in biological tissue [16]. The principle of the probe is based on the measurement of the light induced fluorescence of a ruby sphere [Sandoz SA, Cugy (FR), Switzerland] glued to the end of an optical fiber (Fig. 6). The ruby sphere can be excited by visible light [350–670 nm] coming from all directions in space. Upon excitation, the ruby fluoresces efficiently near 693 nm. A fraction of this fluorescent light is collected by the optical fiber and can be considered as proportional to the true radiant energy fluence rate of the excitation light. Typical angular re-

Fig. 2. Negative imprint in wax of the bronchial tree (dark dots indicate the positions of interest for fluence rate measurement performed with the isotropic detector).

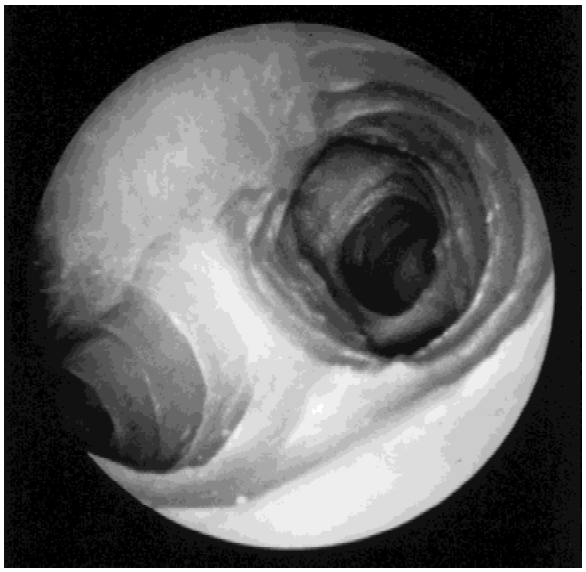

Fig. 3. Endoscopic view of the lung phantom.

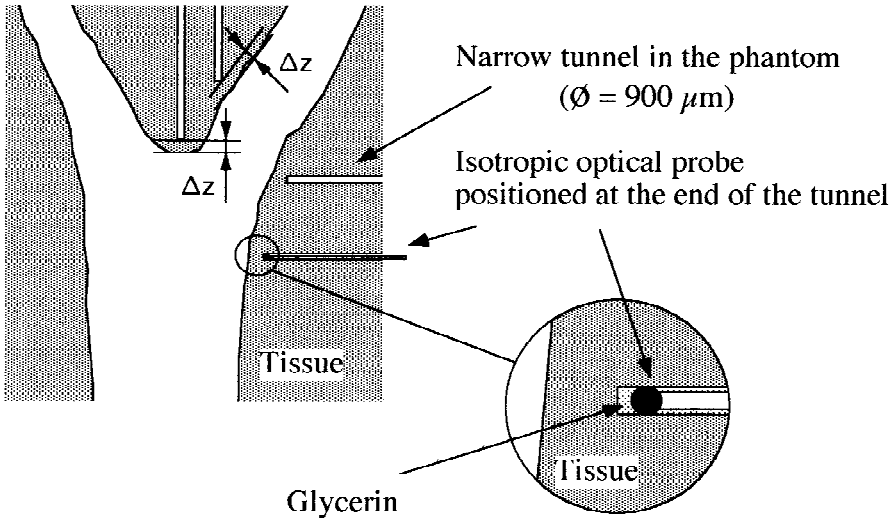

Fig. 4. Narrow tunnels in the silicone phantom through which a thin isotropic optical probe can be introduced in order to measure the radiant energy fluence rate at some positions of interest. The extremity of each tunnel is located at the same distance from the inner surface of the bronchial tree.

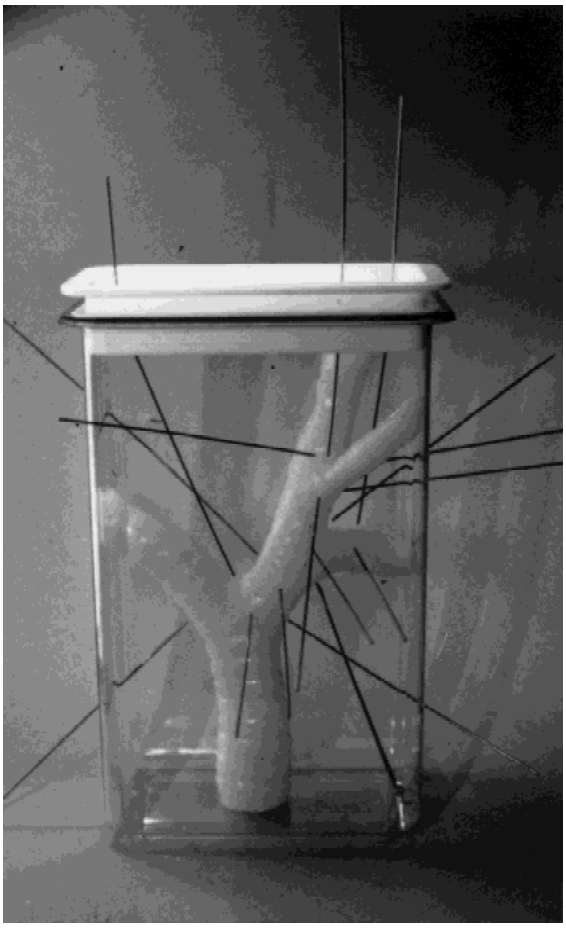

Fig. 5. Steel rods are precisely positioned all around the wax negative imprint of the bronchial tree before immersion in the silicone. After curing, they are withdrawn, leaving tunnels in the phantom.

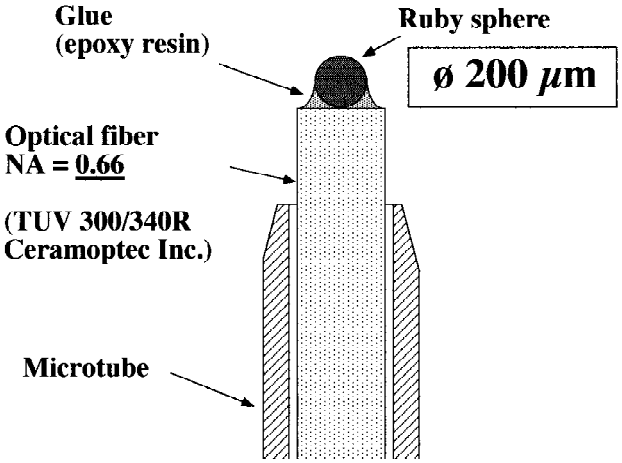

Fig. 6. Schematic diagram of the isotropic optical probe.

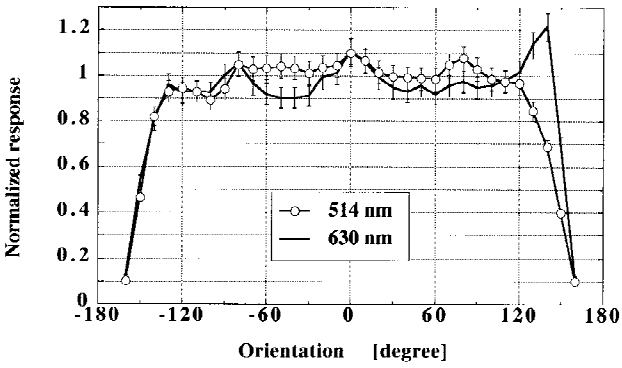

Fig. 7. Typical angular response of the isotropic probe at 514 nm and 630 nm in water.

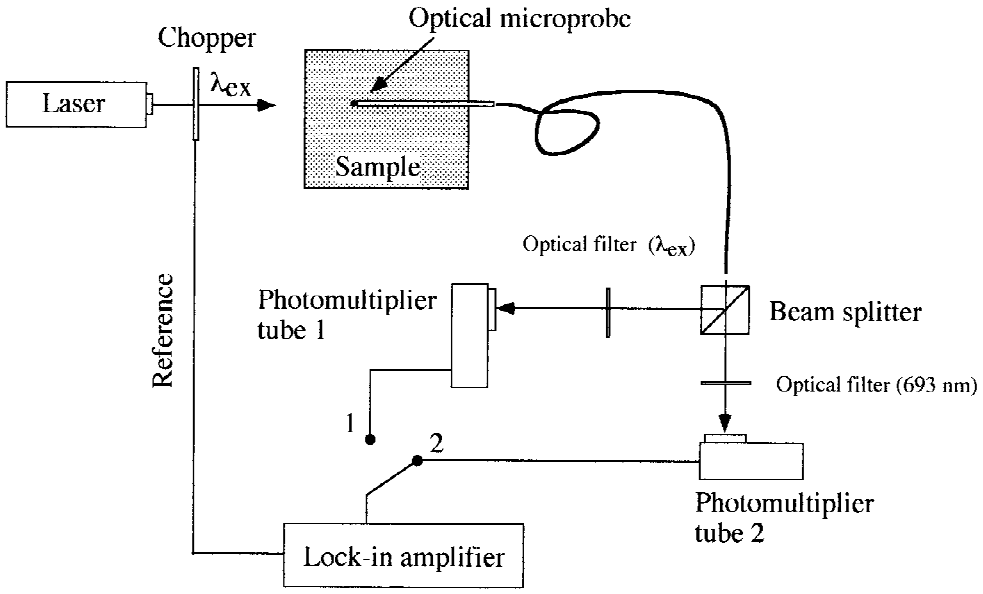

Fig. 8. Schematic diagram of the radiant energy fluence rate measurement with the isotropic ruby probe.

sponses of the fluorescing microprobe at 514 nm and 630 nm, in water (n = 1.33), are shown in Figure 7.

The visible radiation to be measured also causes broad band tissue/phantom autofluorescence which could interfere with the measurement of the isotropic probe [15]. Part of this autofluorescence, near 693 nm, interferes by directly entering the fiber. This contamination can be reduced in the case of a ruby tip by using the difference of fluorescence decay times between ruby and tissue. The ruby fluorescence decay time depends on the Cr^{3+} concentration [17]. The ruby used in our application has a typical value of 2.15 ms. The tissue autofluorescence decay time at 693 nm is much shorter, of the order of 10 ns. Therefore, by using a lock-in technique to detect the fluorescence signal at 693 nm, the tissue autofluorescence and the ruby fluorescence can be easily separated. Indeed, with excitation light with a modulation frequency of more than 465 Hz, the ruby fluorescence signal is about 90° lagging in phase compared to the tissue autofluorescence signal and the excitation light intensity. The broad band tissue autofluorescence can also interfere in the measurement by inducing fluorescence at 693 nm in the ruby sphere. Experiments performed at 630 nm have shown that this contribution is negligible. In particular, it stays smaller than the contribution of the tissue autofluorescence at 693 nm entering directly into the fiber, even if the latter is greatly reduced by the lock-in technique.

The experimental set-up used with the isotropic probe is presented in Figure 8. The light collected by the optical fiber of the isotropic probe is split into two beams. One of the beams is filtered at the light source wavelength and the other one at the ruby fluorescence wavelength. Both light intensities are measured by a photomultiplier tube. The signal corresponding to the light source wavelength can be considered as in phase with the tissue autofluorescence at 693 nm. This signal is consequently used to set-up the phase of the lock-in amplifier before any measurement in order to make the lock-in insensitive to the tissue autofluorescence signal. After this initial procedure, the signal of the ruby fluorescence can be selectively measured by the lock-in amplifier. In the measurements presented hereafter, no other calibration procedure has been performed, since the absolute value of the radiant energy fluence rate was not looked for.

Figure 9 shows typical results of a relative radiant energy fluence rate measurement performed in the lung phantom at 630 nm. The light distributor to be tested was a new light diffuser based on an air-filled silicone balloon with a diffuse reflecting membrane [8]. In order to fit the geometry of the lung spur, the balloon has a "heart" shape. In this application, the measurements allow us to sample the radiant energy flu-

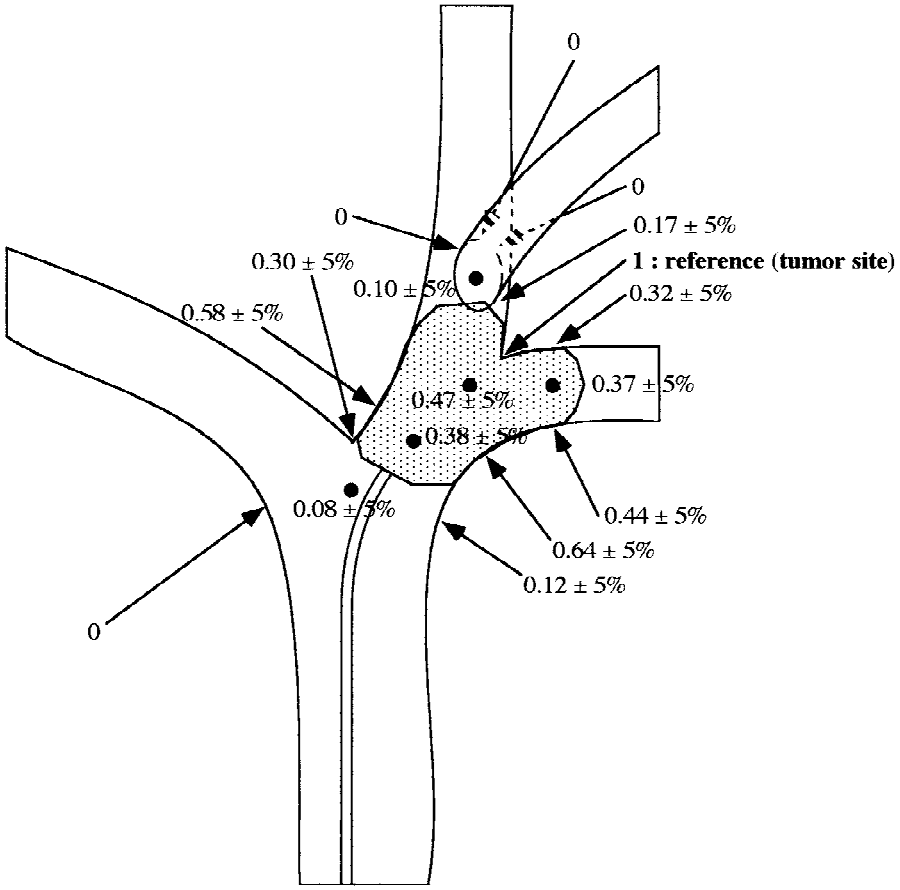

Fig. 9. Relative radiant energy fluence rate measurement performed at several specific positions (see Fig. 2) in the lung phantom with the isotropic probe. A "heart shape" balloon light distributor was used. The radiant energy fluence rate at the tumor site is the reference value. The relative error has been determined by performing several measurements. Between each measurement, the balloon has been removed from the lung phantom and then repositioned.

ence rate at different spatial locations, and thus decide if the light distributor is appropriate for the anatomical site in question. The measurements are also used to evaluate the effect of balloon positioning on the absolute light dosimetry and on the relative distribution of radiant energy fluence rate.

CONCLUSION

Silicone-based optical phantoms have been built which accurately mimic the mechanical and geometrical properties of organs as well as their optical properties. Molding appears to be well suited for the production of any three-dimensional shape. Scattering properties obtained by adding Al_2O_3 particles or polystyrene spheres are homogeneous in such a medium and can be predicted by Mie theory. Absorption and fluorescence properties are obtained by adding suitable pigments or dyes to act as chromophores or fluorophores.

Stable over time and easy to handle, these types of phantoms are efficient tools for photomedicine. They can be used for testing, calibrating, or comparing new devices. As an example, we have shown a three-dimensional optical phantom of the tracheo-bronchial tree which is currently being used to test new light diffusers for PDT in the lung.

ACKNOWLEDGMENTS

The authors are grateful to the Swiss "Fonds National", the Common Research Program in biomedical technology between the Lausanne's Hospital (CHUV), the Swiss Federal Institute of Technology (EPFL), and the Lausanne's Univer-

sity (UNIL); the Swiss National Priority Program in Optics; and Ciba-Geigy for financial support. A. Vitkin also acknowledges support from the National Cancer Institute of Canada (grant to B. Wilson).

REFERENCES

1. Wilson BC, Patterson MS. The physics of photodynamic therapy. Phys Med Biol 1986; 31:327–360.
2. Van den Bergh H. Photodynamic therapy and photodetection of early cancer in the upper aerodigestive tract, the tracheobronchial tree, the oesophagus and the urinary bladder. In: Amaldi U, Larsson B, eds. "Hadrontherapy in Oncology. Proceedings of the First International Symposium on Hadrontherapy." Amsterdam-Lausanne-New York-Oxford-Shannon-Tokyo. Elsevier Science 1994: 577–621.
3. Hayata Y, Konaka C. Photodynamic therapy of neoplastic disease. In: Kessel D, ed. "Photodynamic Therapy of Neoplastic Disease," Vol. 1. Boca Raton: CRC Press, 1990:43–64.
4. Henderson WB, Dougherty TJ. Clinical applications of photodynamic therapy. In: Henderson WB, Dougherty TJ, eds. "Photodynamic Therapy: Basic Principles and Applications." New York, Basel, Hong Kong: Marcel Dekker, Inc., 1992:219–331.
5. Wagnières G, Monnier P, Savary M, Cornaz P, Châtelain A, van den Bergh H. Photodynamic therapy of early cancer in the upper aerodigestive tract and bronchi: instrumentation and clinical results. Proc SPIE 1990; IS 6:249–271.
6. Mizeret J, Thielen P, Theumann JF, Bays R, Wagnières G, Savary JF, Monnier P, van den Bergh H. New distributors for homogeneous and monitorable light delivery in photodynamic therapy. Proc SPIE 1994; 2323:58–69.
7. Mizeret J, van den Bergh H. A cylindrical fiberoptic light diffuser for medical applications. Lasers Surg Med 1996; 159–167.
8. Van den Bergh H, Mizeret J, Theumann JF, Woodtli A, Bays R, Robert D, Thielen P, Philippoz JM, Braichotte D, Forrer M, Savary JF, Monnier Ph, Wagnières G. Light distributors for photodynamic therapy. Proc SPIE, 1996;2631:173–198.
9. Firbank M, Delpy DT. A design for a stable and reproducible phantom for use in near infra-red imaging and spectroscopy. Phys Med Biol 1993; 38:847–853.
10. Bolin FP, Preuss LE. Refractive index of some mammalian tissues using a fiber optic cladding method. Appl Optics 1989; 28:2297–2303.
11. Bohren GR, Huffman DR. "Absorption and Scattering of Light by Small Particles." Appendix A. New York: Wiley-Interscience, 1983.
12. Vitkin IA, Woolsey J, Wilson BC, Anderson RR. Optical and thermal characterization of natural (*Sepia officinalis*) melanin. Photochem Photobiol 1994; 59:455–462.
13. Paine AJ, Luymes W, McNulty J. Dispersion of styrene in polar solvents. 6. Influence of reaction parameters on particle size and molecular weight in poly(N-vinylpyrrolidone)-stabilized reactions. Macromolecules 1990; 23: 3104–3109.
14. Flock ST, Patterson MS, Wilson BC, Wyman DR. Monte Carlo modeling of light propagation in highly scattering tissues—I: Model predictions and comparison with diffusion theory. IEEE Trans Biomed Eng 1989; 36:1162–1168.
15. Bays R, Monnier P, Wagnières G, Braichotte D, van den Bergh H, Burckhardt CW. Clinical optical dose measurement for PDT: invasive and non-invasive techniques. Proc SPIE 1991; 1525:397–408.
16. Bays R, Wagnières G, Robert D, Mizeret J, Braichotte D, Savary JF, Monnier P, van den Bergh H. Clinical measurements of tissue optical properties in the esophagus. Proc SPIE 1995; 2324:39–45.
17. Barthem RB, Abritta T, Eichler JPF, de Souza Barros F. Some properties of the fluorescence spectra of heavily doped ruby. J Luminescence 1982; 27:231–235.